Journal of Atmospheric and Solar–Terrestrial Physics 273 (2025) 106542

Contents lists available at ScienceDirect

Journal of Atmospheric and Solar-Terrestrial Physics

journal homepage: www.elsevier.com/locate/jastp

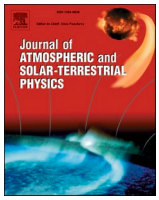

Research Paper

Study of rotational temperatures with a multi-wavelength photometer from the Indian equatorial station Tirunelveli

Sukanta Sau [a,*], S. Gurubaran [b], V.L. Narayanan [c], Dupinder Singh [d], S. Sripathi [a], A.P. Dimri [b]

[a] Equatorial Geophysical Research Laboratory, Indian Institute of Geomagnetism, Krishnapuram, Tirunelveli, 627011, India
[b] Indian Institute of Geomagnetism, Plot No. 5, Sector 18, New Panvel (W), Navi Mumbai, 410218, India
[c] Krea University, Sri City, Andhra Pradesh, 517646, India
[d] MIT Haystack Observatory, 99 Millstone Road, Westford, MA, 01886, USA

ARTICLE INFO

Handling editor: Dora Pancheva

Keywords:
Multi-wavelength photometer
Mesosphere lower thermosphere (MLT)
Hydroxyl nightglow emission
SABER onboard TIMED satellite
Photometer and SABER temperature comparison
MLT temperature variabilities

ABSTRACT

A multi-wavelength photometer (MWP) was operated at the equatorial station Tirunelveli (8.7°N, 77.8°E geographic), India, to study different nightglow emissions. In the present work, the intensities of the P1(2) and P1(4) lines of the OH(6,2) Meinel band were used to derive rotational temperatures in the mesosphere-lower thermosphere (MLT) region during February–April 2015. The methodology adopted to derive rotational temperatures using the MWP data is discussed in detail. A comparison with temperatures measured by the Sounding of the Atmosphere by Broadband Emission Radiometry (SABER) instrument onboard NASA's TIMED satellite was performed to validate the MWP-derived rotational temperatures. An excellent correlation was observed between the MWP-derived and SABER temperatures, with a mean temperature difference of ~15 K. The plausible reasons for this temperature bias are discussed in this work. In addition, the P1 line intensities of the OH(6,2) band and temperatures obtained with the MWP were compared with the OH broadband intensity acquired by a co-located all-sky airglow imager (ASAI). Furthermore, the local time variation of the MWP-derived temperatures was studied, and the results were compared with the NRLMSISE-00 model simulation. This study demonstrates the effectiveness of the MWP in measuring MLT temperatures and highlights the importance of multi-instrument comparisons for validating the temperatures and airglow intensity.

1. Introduction

One of the most dynamic regions of the Earth's atmosphere is the mesosphere-lower thermosphere (MLT) region. This region is influenced by various forcings from below, such as tides, planetary waves, and gravity waves (GWs) generated by convective activities, orography, and fronts, as well as forcings from above, such as variability in the solar activity level, geomagnetic disturbances, etc. The background parameters (mainly wind and temperature) of the MLT region play an important role in the vertical and horizontal propagation of GWs. Many of these GWs dissipate their energy and momentum in the MLT region, which in turn modulates the background parameters of the MLT region and aids in generating secondary or higher-order GWs. Therefore, it is of utmost importance to study the background parameters of the MLT region to gain a better understanding of vertical coupling in the atmosphere.

Historically, measuring temperatures in the MLT region has been challenging. This region is too low for in-situ satellite measurements and too high for balloon soundings to reach. Multiple low-earth orbiting satellite missions over the past few decades have provided a valuable database of MLT temperatures (e.g., García-Comas et al., 2014; Reid et al., 2017). Although these satellites offer excellent spatial coverage globally, their temporal coverage at any specific location is quite limited. For this reason, ground-based instruments are crucial for obtaining continuous measurements at any location. Various ground-based instruments, such as meteor radars and lidars, have been employed across different latitude-longitude sectors to study MLT temperatures (Nozawa et al., 2023; Reid, 2024; Yue et al., 2019). Another class of widely used ground-based instruments for studying MLT temperatures is the passive optical instruments, such as photometers (Meriwether, 1975), all-sky airglow imagers (Taylor et al., 2005), spectrometers (Sau et al., 2024) and interferometers (Wiens et al., 1997).

Photometers have been widely used across different latitude-longitude sectors to derive MLT temperatures over the last few

* Corresponding author.
E-mail address: sukanta.s@iigm.res.in (S. Sau).

https://doi.org/10.1016/j.jastp.2025.106542
Received 2 December 2024; Received in revised form 1 May 2025; Accepted 15 May 2025
Available online 16 May 2025

decades (Meriwether, 1975; Scheer, 1995; Takahashi et al., 1994; Tepley et al., 1981). These temperatures are utilized to study atmospheric tides, GWs, and planetary waves in the MLT region as well as short- and long-term MLT variabilities. Extensive research on MLT dynamics has been carried out at various locations in India using temperatures obtained with ground-based photometers (Ghodpage et al., 2019; Guharay et al., 2009; Mukherjee and Parihar, 2004; Parihar et al., 2017; Taori et al., 2012a). Several studies have focused on the daytime MLT dynamics across India, including the equatorial region (e.g., Sridharan et al., 1999; Vineeth et al., 2011). However, investigation of the nighttime MLT dynamics using temperatures estimated from ground-based airglow observations is lacking in the Indian equatorial sector.

For the reason mentioned above, an MWP was installed by the Indian Institute of Geomagnetism at its equatorial station in Tirunelveli (8.7° N, 77.8° E). In this work, we have discussed in detail the methodology to estimate rotational temperatures using the MWP data. Before applying MWP-derived temperatures (henceforth MWP temperatures) in MLT studies, it is important to validate them. This is accomplished by comparing the MWP temperatures with measurements from the SABER instrument on board the TIMED satellite. We then discuss the probable reasons that could cause the temperature difference between these two instruments. In addition, we have compared the P1 line intensities of the OH(6,2) band and temperatures obtained using the MWP with the OH broadband intensity acquired by a co-located ASAI as an additional validation step. Following this, we have discussed the local time variation of the MWP temperatures during the study period (February–April 2015) and compared the results with the NRLMSISE-00 model simulation.

2. Instruments

In this work, we have used data from three instruments which are described below.

2.1. Multi-wavelength photometer

The optical design of the MWP is similar to the photometer utilized by Taori et al. (2012a) and it employs an f/2 optical system. A convex lens with a diameter of 100 mm acts as the front-end lens and gathers the incoming flux of airglow emissions. A mirror assembly is mounted above the front-end lens so as to allow the instrument to point at different azimuthal positions and elevation angles. There is an arrangement to place a circular aperture of variable diameter at the focal point of the front-end lens. The size of the circular aperture determines the field of view (FoV) of the instrument. During our study period, an aperture having a 3 mm diameter was used, yielding a field of view (FoV) of ~4°. A collimating lens of 50 mm diameter is placed below the circular aperture to render parallel rays on the interference filters. The light transmitted through the filter assembly is focused on the detector using another lens with a diameter of 50 mm. A Hamamatsu H7421-50 series photomultiplier tube (PMT) serves as the detector for the MWP. This PMT consists of a GaAs photocathode, which enables detection over a wide spectral range from 380 nm to 890 nm. The PMT has a low dark count (~125 counts/s within 5°–35 °C) and high count sensitivity (~3.9 $\times$ 10^5 $s^{-1}pW^{-1}$ at 800 nm). The PMT is equipped with a counting unit that uses a USB interface to communicate to a computer. The operation of the MWP and data acquisition are carried out using a software interface. A schematic diagram and a photograph of the Tirunelveli MWP are shown in Fig. 1.

The MWP contains seven interference filters housed on a filter wheel inside a temperature-controlled chamber. A set of 16 Peltier elements and a proportional integral derivative (PID) controller are used to control the temperature of the filter chamber with a precision of better than 0.25 °C. The filter wheel is rotated using a motor to align the filters along the optical axis of the instrument. There are two magnetic sensors above the filter wheel. One of the sensors helps to locate the filter position while the other one tracks the rotation of the filters. Details of the interference filters accommodated in the MWP are provided in Table 1.

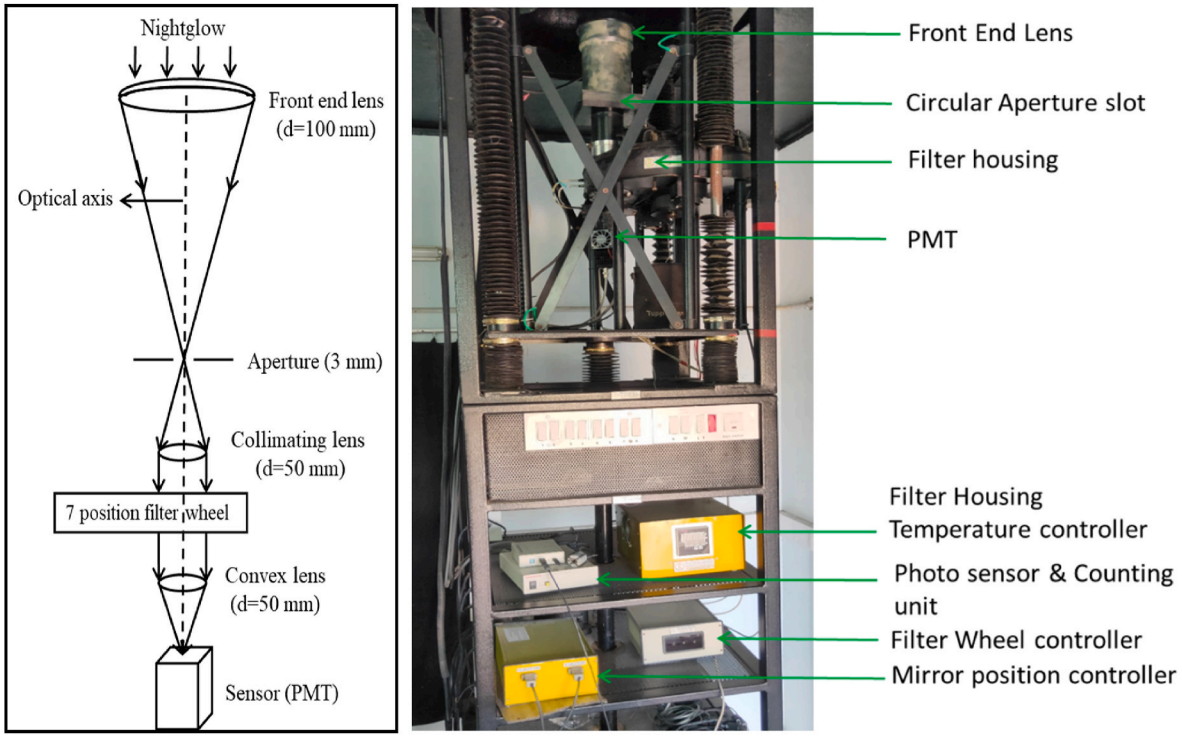

Fig. 1. (Left) A schematic diagram of the Tirunelveli MWP. The diameters of the lenses and the circular aperture are mentioned inside brackets. (Right) A photograph of the Tirunelveli MWP. All the major components of the MWP are noted to the right of the photograph.

Table 1
Details of the interference filters accommodated in the Tirunelveli MWP.

Filter wheel Sequence	Filter Description	Central wavelength (nm)	Bandwidth (nm)	Average Centroid Emission Altitude (km)
1	OI Redline Emission	630.0	0.5	250
2	Background for the O_2(0,1) band	857.0	0.4	–
3	P branch line, O_2(0,1) band	865.5	0.4	94
4	P branch line, O_2(0,1) band	867.5	0.4	94
5	P1(2) line, OH (6,2) band	839.92	0.5	87
6	P1(4) line, OH (6,2) band	846.53	0.5	87
7	Background for the OH(6,2) band	845.8	0.5	–

2.2. SABER

This study utilizes SABER version 2.07 data for kinetic temperatures and volume emission rate (VER) of OH emission. SABER retrieves kinetic temperatures from observations of CO_2 limb emission at 15 μm wavelength. It has been shown that the uncertainties in the SABER kinetic temperatures are within ±1.5 K below 95 km altitude (García-Comas et al., 2008). SABER measures OH VER at 2.0 μm (channel A) and 1.6 μm (channel B) wavelengths. The 2.0 μm VER consists of line emissions from the OH(9,7) and OH(8,6) bands, while the 1.6 μm VER includes the OH (5,3) and OH(4,2) bands. SABER provides kinetic temperatures and OH VER data at an altitude interval of ~0.4 km between 80 km and 95 km altitude. Further information on the SABER instrument can be found in Russell et al. (1994) and Esplin et al. (2023). Previous studies have reported the SABER-derived temperatures to be very reliable and stable with time (e.g., Dawkins et al., 2018; Mertens et al., 2001; Mlynczak et al., 2020).

2.3. All-sky airglow imager

An ASAI was installed at Tirunelveli in 2007 to measure various nightglow emissions and was operated till July 2016. This instrument is equipped with a Mamiya fisheye lens at the front, providing a 180° field of view (FoV). However, the FoV of the ASAI was restricted to 140° during the present study period to minimize light pollution from vehicle movements on the nearby road. Seven interference filters are housed inside a temperature-controlled chamber to measure different nightglow emissions. A charge-coupled device (CCD) having 512 × 512 pixels and 16-bit depth captures the nightglow photons. The CCD was cooled to −75 °C to minimize background thermionic emissions. Further details about the Tirunelveli ASAI can be found in Narayanan et al. (2009b). This study utilizes data obtained with a broadband (705–928 nm) OH filter with a notch at 865 nm to suppress atmospheric O_2(0,1) band emission. Images obtained with the broadband OH filter at Tirunelveli have been used to study atmospheric gravity waves and mesospheric bore. The high spatial resolution and sensitivity of the Tirunelveli ASAI enabled it to capture even the small-scale mesospheric ripples (Narayanan and Gurubaran, 2013; Narayanan et al., 2009a, 2010, 2012).

3. Data and methodology

In this work, we have utilized intensities of the P1(2) and P1(4) lines of the OH(6,2) Meinel band and their corresponding background data measured by the Tirunelveli MWP. The instrument was operated between January 2015 and July 2016. Data obtained during February–April 2015 were analyzed for validation purposes. The MWP was operated on 23 nights during the study period, with good quality data available for ~116 h. Data were obtained on seven nights during February (winter), while during the spring months of March and April, data were recorded on 11 and 5 nights, respectively. Since the PMT of the MWP has not been calibrated against a known brightness source, counts obtained from each filter are considered to represent the intensities of the respective nightglow emissions along with the background skylight. The filter centered at 845.8 nm measures the background skylight for the OH(6,2) band.

During the study period, an integration time of 10 s per data point was used for all the filters. Two different routines were adapted to collect the data. In the first (second) routine, three (two) consecutive measurements were obtained for each filter in a data cycle. In the initial period of operation (which includes February 2015), the first routine was adopted. As it takes less time (~10 s less) to obtain two consecutive measurements per filter, we adopted the second routine in March 2015 and thereafter. For ease of analysis, we averaged these consecutive measurements to obtain an average count for each filter in a data cycle. These average counts for the P1(2), P1(4), and OH(6,2) background filters are utilized in further analysis.

3.1. Estimation of rotational temperatures using Tirunelveli MWP data

Estimation of rotational temperatures using the P1 line intensities of the OH(6,2) band is based on the assumption that these lines follow the Boltzmann distribution. Further, the MWP temperatures can represent atmospheric temperatures only under the assumption of local thermodynamic equilibrium (LTE). Considering the collision frequency and lifetime of the excited hydroxyl molecules (OH*), these two conditions are expected to be satisfied (Pendleton Jr. et al., 1993). Based on this assumption, the intensity (I) of the P1 lines of the OH(6,2) band can be expressed as

$$I_{v',J'\rightarrow v'',J''} = N_{v'} A_{v',J'\rightarrow v'',J''} \left[\frac{2(2J'+1)hcB_v}{k_B T_r}\right] \cdot \exp\left(-\frac{F(J')hc}{k_B T_r}\right) \quad (1)$$

Here, v' and J' (v'' and J'') represent the vibrational and rotational quantum numbers of the upper (lower) energy level. $N_{v'}$ is the total concentration of OH* molecules at the vibrational level v'. The term $A_{v',J'\rightarrow v'',J''}$ (henceforth denoted by A) represents the Einstein coefficient for a particular line transition. The symbols h, c, k_B, and T_r stand for Planck's constant, speed of light in free space, Boltzmann constant, and the rotational temperature, respectively. The rotational constant B_v and rotational term $F(J')$ are obtained following Krassovsky et al. (1962).

In this study, we have used the well-established ratio method that utilizes the intensities of two rotational lines of any OH band to estimate rotational temperatures (Meriwether, 1975; Takahashi et al., 1974). By taking the ratio of the P1(2) and P1(4) line intensities of the OH(6,2) band, and rearranging the terms, the rotational temperature can be expressed as

$$T_r = \frac{\frac{hc}{k_B}\left(F(J'_2) - F(J'_1)\right)}{\ln\left(\frac{A_2 I_1 (2J'_2+1)}{A_1 I_2 (2J'_1+1)}\right)} \quad (2)$$

In Equation (2), the subscripts 1 and 2 represent rotational constants and coefficients for P1(2) and P1(4) lines of the OH(6,2) band, respectively. By evaluating all the terms of Equation (2), we obtain the final expression for the rotational temperature, which depends only on the ratio of the P1(2) and P1(4) line intensities.

$$T_r \cong \frac{228.6}{\ln\left(2.6905 \cdot \frac{I_1}{I_2}\right)} \quad (3)$$

In this work, the Einstein coefficients for line transitions are adapted from Langhoff et al. (1986), as previous studies have shown that these sets of coefficients produce the most realistic rotational temperatures (Sau et al., 2024). To estimate the ratio $\frac{I_1}{I_2}$, we have utilized background subtracted P1(2) and P1(4) line counts. The typical uncertainty in the MWP temperatures is found to be in the range of 2–6 K. The temporal variation of the background subtracted P1(2) and P1(4) line counts and the rotational temperatures estimated using them on 19 February 2015 are shown in Fig. 2. In this work, the date 19 February 2015 denotes the period between 18:00 IST on 19 February 2015 and 06:00 IST on 20 February 2015 unless specified otherwise, and this convention applies to all the dates mentioned here.

3.2. Estimation of weighted temperatures from SABER data

SABER provides altitude-resolved temperature measurements while MWP temperatures are naturally weighted by the OH(6,2) band VER. Therefore, to compare SABER and MWP temperatures, it is essential to weight the SABER temperature profiles with the OH(6,2) band VER (Sau et al., 2024). Since direct measurements of the OH(6,2) band VER profile were unavailable, we have utilized the OH VER profiles recorded by SABER in this work. Previous studies have shown that OH emissions at higher vibrational levels possess higher VER peak altitudes (von Savigny et al., 2012). Considering the OH bands that constitute SABER 1.6 μm and 2.0 μm channels, it is expected that the peak altitude of the OH(6,2) band VER will be situated between the peak altitudes of the 1.6 μm and 2.0 μm VER.

As a next step, SABER 1.6 μm and 2.0 μm VER profiles are normalized with respect to their peak VERs. The range of altitudes having normalized VER $\geq$0.5 constitutes the weighting function for both the 1.6 μm and 2.0 μm channels. The weighted SABER temperatures obtained by applying the normalized 1.6 μm and 2.0 μm VER profiles will henceforth be denoted by $T_{1.6}$ and $T_{2.0}$, respectively. In this work, an average of $T_{1.6}$ and $T_{2.0}$ has been considered as the OH(6,2) band equivalent temperature from SABER (denoted by T_m) since the peak of the OH(6,2) band VER is expected to be between peaks of 1.6 μm and 2.0 μm VER.

4. Results and discussion

4.1. Comparison between MWP and SABER temperatures

We have compared MWP temperatures with T_m to validate the former. During the study period, the MWP was pointed at a 30° elevation angle either to the north or to the south of Tirunelveli. All the SABER passes available within ±3° latitude-longitude of the MWP target locations are considered in the analysis. The mean of all the MWP temperatures available within ±5 min of the average time of the SABER pass inside the target area is considered in the comparison. The spatial and temporal criteria mentioned above are satisfied on only five nights. We have plotted the T_m values as a function of the average MWP temperatures in Fig. 3. An excellent correlation is obtained between these two temperature sets (Fig. 3) while their average temperature difference is 14.88 ± 4.31 K. Details of the comparison are summarized in Table 2.

4.1.1. Comparison of results with previous studies

A few earlier studies have compared SABER temperatures in the MLT region with rotational temperatures obtained from ground-based OH emission measurements during nighttime. Oberheide et al. (2006) used a Czerny-Turner spectrometer to measure OH(3,1) band emission from Wuppertal (51.3° N, 7.1° E) over three years. They found that, on average, the OH(3,1) rotational temperatures were greater (warmer) than the weighted SABER temperatures by 7.5 K. López-González et al. (2007) compared four years of weighted SABER temperatures with OH (6,2) rotational temperatures estimated by an imaging Fabry-Perot spectrometer operated at Sierra Nevada (37.1° N, 3.4° W) and observed a mean warm bias of 5.7 K in the OH(6,2) rotational temperatures. Mulligan and Lowe (2008) utilized two years of Fourier transform infrared spectrometer from Maynooth (53.2° N, 6.4° W), and Ebert-Fastie spectrometer data from Wuppertal to estimate OH(3,1) rotational temperatures. They reported that the OH(3,1) rotational temperatures were greater than the weighted SABER temperatures by 8.6 K and 4.5 K at Maynooth and Wuppertal, respectively. Liu et al. (2015) analyzed three years of Czerny-Turner spectrometer data obtained from Xinglong (40.2° N, 117.4° E) and found that on average, the OH ($v = 6$) rotational temperatures were 2.7 K warmer than the weighted SABER temperatures. By comparing weighted SABER temperatures with OH(6,2) rotational temperatures obtained from an Ebert-Fastie spectrometer operated at Arecibo (18.4° N, 66.8° W), Sau et al. (2024) observed the OH(6,2) rotational temperatures to be colder than the SABER temperatures by 15.6 K.

In the Indian longitude sector, Guharay et al. (2009) compared one night of OH(6,2) temperatures estimated by a multi-filter photometer operated at Nainital (29.4° N, 79.5° E) with SABER temperatures. They observed the OH(6,2) temperature to be 2 K colder than the weighted SABER temperature. Using a few nights of multi-filter photometer observation from the low-latitude station Gadanki (13.5° N, 79.2° E), two comparative studies were conducted between the OH(6,2) and SABER temperatures (Taori et al., 2011, 2012b). They reported both

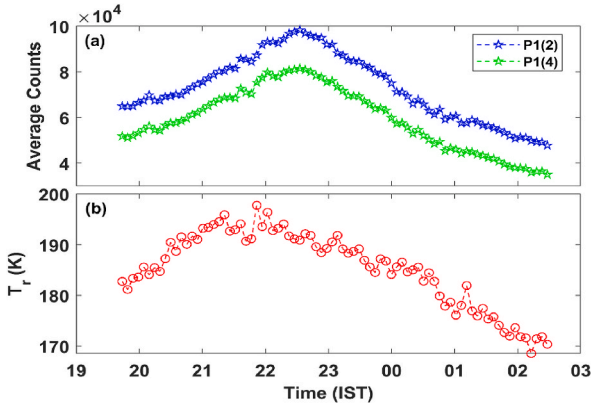

Fig. 2. (a) Average counts of the P1(2) and P1(4) lines of the OH(6,2) band on the night of 19 February 2015. Blue and green colors stand for the P1(2) and P1(4) lines, respectively. (b) Temporal variation of the rotational temperatures (T_r) obtained by using the ratio of the P1(2) and P1(4) counts shown in panel (a) of this Figure.

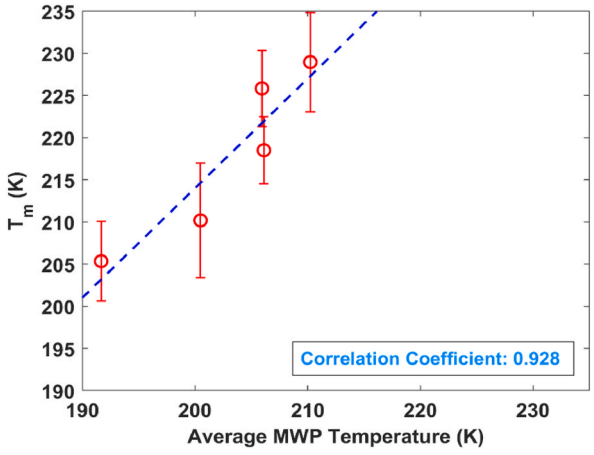

Fig. 3. Plot of T_m as a function of the average MWP temperatures. The red open circles and red vertical lines represent T_m values and one standard deviation in T_m, respectively. The blue dashed line is the linear fit between these two temperature sets.

Table 2
Details of the comparison between SABER and MWP temperatures. Each row in the $T_{1.6}$ and $T_{2.0}$ columns corresponds to one temperature profile of SABER.

Date (ddmmyyyy)	Approximate Time of SABER pass (IST)	$T_{1.6}$ (K)	$T_{2.0}$ (K)	T_m (K)	Average MWP Temp. (K)	(T_m – MWP) Temp (K)
18032015	23:57	230.14	228.78	225.84	205.94	19.90
		224.14	220.28			
20032015	00:10	208.89	209.96	205.34	191.67	13.67
		201.07	201.46			
22032015	23:13	236.59	229.52	228.97	210.24	18.73
		227.36	222.40			
23032015	23:26	223.57	219.3	218.50	206.12	12.38
		216.97	214.18			
23042015	01:44	207.25	201.01	210.18	200.48	9.70
		211.05	206.22			
		219.68	215.88			

warm and cold biases of 1–4 K and 8 K, respectively, in the OH(6,2) temperatures. Parihar et al. (2017) analyzed three years of multi-filter all-sky imager data taken from Ranchi (23.3° N, 85.3° E) and found that on average, the OH(6,2) temperatures were 4–5 K warmer than the weighted SABER temperatures.

It can be noted from the preceding discussion that both warm and cold biases are reported in the OH rotational temperatures with respect to the SABER temperatures. However, a warm bias appears more prevalent in the OH rotational temperatures, specifically over mid-latitudes. Over low latitudes, past results seem to show both warm and cold biases in different studies. It is evident from Fig. 3 and Table 2 that Tirunelveli MWP temperatures are colder than T_m. Thus, our result is similar to the findings of Guharay et al. (2009), Taori et al. (2011), and Sau et al. (2024), and is opposite to the general trend of a warm bias. The mean difference between the OH(6,2) and SABER temperatures obtained in the present study is larger than most previous studies, except for Sau et al. (2024). It is interesting to note that all the comparison studies utilizing a large (~few years) database have reported a warm bias in the ground-based OH temperatures over the SABER temperatures (e.g., Liu et al., 2015; López-González et al., 2007; Mulligan and Lowe, 2008; Oberheide et al., 2006; Parihar et al., 2017), while a cold bias is observed when using a much smaller (~ few days) database (e.g., Guharay et al., 2009; Sau et al., 2024; Taori et al., 2011). In the case of a large database, the mean temperature difference is obtained by averaging a large number of individual temperature differences. Typically, these individual temperature differences are in the range of ±20 K, and in certain cases, differences greater than 20 K have also been reported (e.g., Liu et al., 2015; López-González et al., 2007; Oberheide et al., 2006; Parihar et al., 2017; Sau et al., 2024). In the present study, only five individual temperature differences are available (Table 2) and this small sample size could be one of the reasons for the large mean temperature difference. A comparative study using a much larger database is required to have a better estimate of the bias between the MWP and SABER temperatures.

4.1.2. Possible factors that influence MWP and SABER temperature comparison

It is a common practice to compare temperatures retrieved from ground-based airglow intensity measurements with those from satellites to validate the ground-based measurements (e.g., Mulligan and Lowe, 2008; Sau et al., 2024; Smith et al., 2010). However, it is important to consider potential factors that could contribute to any discrepancies or bias between these two sets of temperatures, apart from the sample size considered in the analysis. The MWP has a very narrow FoV (~7 × 7 km^2) while SABER possesses a much larger FoV (~4000 km^2). Therefore, the temperature fields observed by MWP and SABER could be affected by waves of different spatial scales, leading to a larger temperature difference between them. As mentioned earlier, the estimation of rotational temperatures using the MWP data relies on the assumption of LTE, while non-LTE conditions are considered in the SABER temperature retrieval algorithm (Mertens et al., 2001). It is not apparent whether this fundamental difference in the temperature estimation methodology causes a temperature difference between the two instruments.

It has been shown previously that large uncertainties (~± 8 K at 90 km altitude) could occur in the SABER kinetic temperatures in the presence of large vertical gradients in temperatures (García-Comas et al., 2008). Several mechanisms could induce a large vertical temperature gradient in the MLT region, such as a temperature inversion layer, tidal activity, etc. Further, García-Comas et al. (2008) have found that when a temperature inversion layer is present in the MLT region, the maximum temperature uncertainty occurs around the crest or trough of the inversion. Parihar et al. (2017) reported large differences (~11–15.5 K) between the MLT temperatures estimated with a ground-based all-sky imager and SABER whenever the peak of the SABER OH 2.0 μm VER was situated close to the crest of a temperature inversion. They also observed that temperature differences between these two instruments were less when the peak of the SABER OH 2.0 μm VER was away from the crest of the temperature inversion layer.

An investigation of the SABER kinetic temperature profiles used in the present study reveals that temperature inversion layers were present on all five nights mentioned in Table 2. The largest vertical temperature gradients were observed on 18 and 22 March 2015 (Fig. 4a and c). The peaks of OH 1.6 μm and 2.0 μm VER on both these nights are situated close to the crests of the temperature inversion. It is apparent from Table 2 that very large temperature differences between MWP and SABER occurred on these two nights. On the night of 19 March 2015, a two-peak temperature inversion layer was observed and the temperature gradient was smaller in comparison to 18 and 22 March 2015. Also, the peaks of OH 1.6 μm and 2.0 μm VER were located below the largest peak of temperature inversion on 19 March 2015 (Fig. 4b). The temperature inversion on the night of 22 April 2015 was smaller in comparison to the other three nights. The peaks of OH 1.6 μm and 2.0 μm VER were located in a region where wavelike features having small temperature gradients were present (Fig. 4d). It is interesting to note that the temperature difference on 19 March 2015 was much smaller than on 18 and 22 March 2015 and the smallest temperature difference in this study was observed on 22 April 2015 (Table 2). Therefore, large temperature differences are observed when the peaks of OH 1.6 μm and 2.0 μm VER are located close to the crests of temperature inversion, and temperature differences are larger when the temperature gradients of the inversions are greater. In addition, Parihar et al. (2017) observed that the ground-based MLT temperatures are always lower than OH equivalent temperatures obtained from SABER whenever a temperature inversion exists, which is similar to the results of this present study.

We wish to mention here that previous studies on mesospheric inversion layers (MILs) from the Indian low and tropical latitude sectors have reported the presence of two distinct MILs. The average lower and upper MIL peak altitudes are around 75 km and 90 km, respectively. The nighttime upper MILs are observed to be more prevalent around the equinoxes in the Indian low-latitude sectors (Fadnavis and Beig, 2004; Ramesh et al., 2017; Sivakandan et al., 2014). It is interesting to note

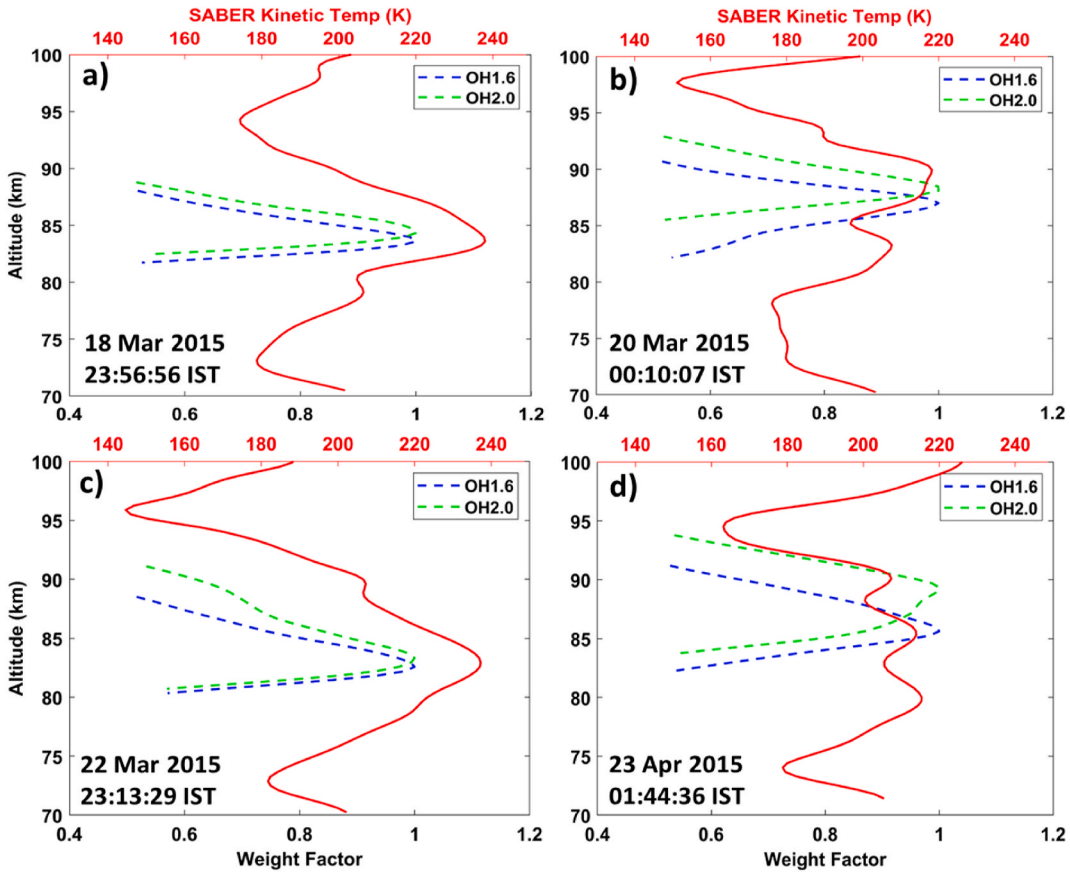

Fig. 4. Plot of SABER kinetic temperatures (solid red line) with altitude. Normalized VER profiles of SABER OH 1.6 μm and 2.0 μm are denoted by dashed blue and green lines, respectively. The range of normalized VERs is fixed between 0.5 and 1.

that observations used in this study were collected predominantly during spring equinox conditions. Therefore, the outcomes of the present study and Parihar et al. (2017) support the findings of García-Comas et al. (2008) that large uncertainties may be present in the SABER temperatures close to the crests of temperature inversions. Considering all the points discussed above and uncertainties in the MWP and SABER temperatures, we believe the MWP temperatures compare fairly well with the SABER temperatures, especially since the correlation coefficient shown in Fig. 3 is rather high at 0.928. This establishes the validity of the MWP temperatures.

4.2. Comparison between Tirunelveli MWP and ASAI data

First, we have compared the intensity of the P1(2) line of the OH(6,2) band obtained using the Tirunelveli MWP with the OH broadband intensity recorded by the co-located ASAI on 19 February 2015. On this night, the MWP was pointed at 30° elevation to the south of Tirunelveli. To estimate the OH broadband intensity equivalent to the MWP intensity, we averaged the intensities of those pixels in an OH broadband image that were within the FoV of the MWP (Fig. 5a). On 19 February 2015, ASAI recorded a set of three consecutive images at an alternate

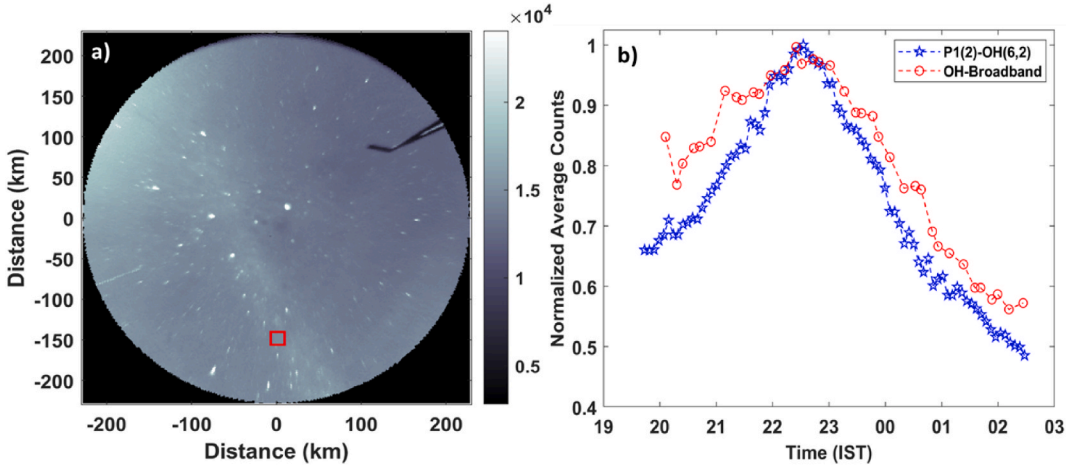

Fig. 5. (a) An unwrapped all-sky image obtained using the OH broadband filter at Tirunelveli on 19 February 2015. The red square denotes the approximate FoV of the MWP. (b) Temporal variations of normalized intensities of the P1(2) line of the OH(6,2) band and the mean OH broadband on 19 February 2015.

cadence of 4 min and 10 min. An integration time of 60 s was used to acquire each image. The OH broadband intensity corresponding to three consecutive images was further averaged to obtain a mean OH broadband intensity. Since the MWP and ASAI had different uncalibrated sensors and integration periods, the intensities of the P1(2) line of the OH(6,2) band and those of the OH broadband were of different magnitudes. Therefore, the intensities of these two instruments were normalized with respect to their peaks for a better comparison (Fig. 5b). It is evident from Fig. 5b that the temporal variation of the MWP and ASAI intensities, as well as the occurrence of their peak intensities, match very well. This result validates the intensities measured by the MWP.

Next, we performed spectral analysis of the mean OH broadband intensities (Fig. 5b) and MWP temperatures (Fig. 2b) obtained on 19 February 2015 to find out the dominant periodicities in them. We calculated the residuals of these two parameters by removing the 1-h running mean from them (Fig. 6a and c). Lomb-Scargle periodograms generated from the residuals of both parameters (Fig. 6b and d) show that the peak power is present at a period of ~39 min for both parameters. Therefore, it is apparent that the OH broadband intensity and MWP temperature can detect the same wave activity. A detailed study will be carried out in the future using a larger database of Tirunelveli OH broadband images and MWP temperatures when data from both instruments are available simultaneously.

4.3. Variabilities in MWP temperatures

Tirunelveli MWP temperatures obtained on different nights during the study period are shown in Fig. 7, with each panel representing a particular month. Here, we have only considered temperatures obtained under cloud-free conditions. MWP temperatures for any single night are indicated by a specific color, as noted in the legend of each panel. Fig. 7 clearly shows significant day-to-day variability in the magnitude and trend of the MWP temperatures over Tirunelveli. Individual temperatures ranging from 135 K to 215 K were observed during the study period. The MWP was oriented at a 30° elevation to the south between 14 February 2015 and 20 March 2015, while it was pointed at 30° elevation to the north between 21 March 2015 and 23 April 2015. On 15 February 2015, the MWP was briefly pointed toward the zenith from 20:08 to 21:30 IST, after which it was directed at a 30° elevation to the south for the remainder of the night.

MWP temperatures for each month were averaged at 30 min intervals. The local time variation of these half-hourly average temperatures will henceforth be referred to as the mean temporal variation (MTV). During April 2015, MWP temperatures were available in the premidnight-midnight sector on one night and in the postmidnight sector on another night (Fig. 7c). Due to this insufficient data, the MTV for this month is not shown in Fig. 7c. Also, it should be noted that the MTV after 04:30 IST in February 2015 (Fig. 7a) follows the temperatures on 21 February 2015, as temperatures were unavailable on other nights during this period. MTVs during February and March 2015 indicate that temperatures gradually increase between evening and midnight, while they decrease gradually after midnight till early morning. The peak temperature was observed at ~23:30 IST in February and March 2015. We have also computed nocturnal mean temperatures during the study period, with observed values ranging from 180 K to 210 K. In Fig. 8, large standard deviations on some nights indicate the presence of strong variabilities in the MLT region, most likely due to wave and/or tidal activities. No apparent trend in the nocturnal mean temperatures was observed with respect to day number (Fig. 8).

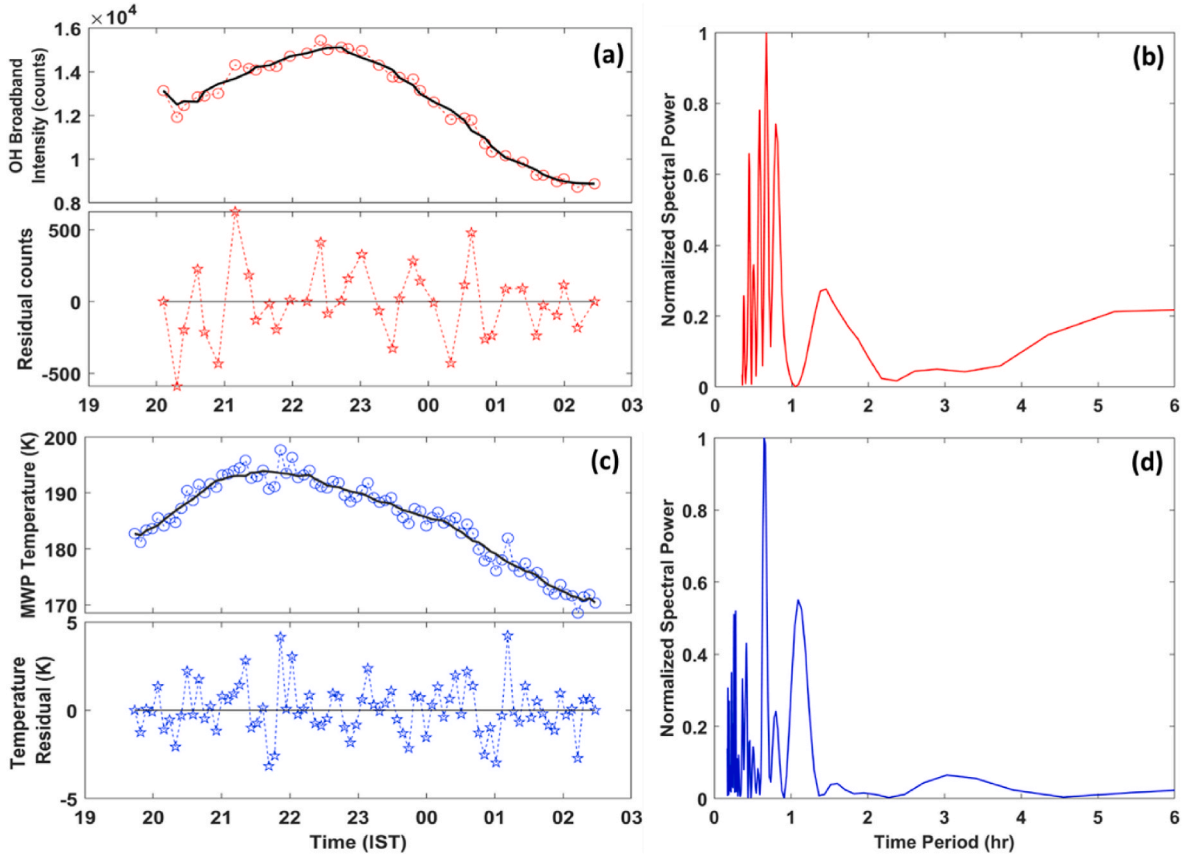

Fig. 6. (a) Temporal variation of the mean OH broadband intensity on 19 February 2015 is denoted by open red circles. The thick black line denotes the 1-h running mean. Residual OH broadband intensities are shown by the red stars. (b) Lomb Scargle periodogram of the residual intensity shown in panel (a) of this Figure. (c) Same as in panel (a) of this Figure but for the MWP temperatures. (d) Lomb Scargle periodogram of the residual MWP temperatures shown in panel (c) of this Figure.

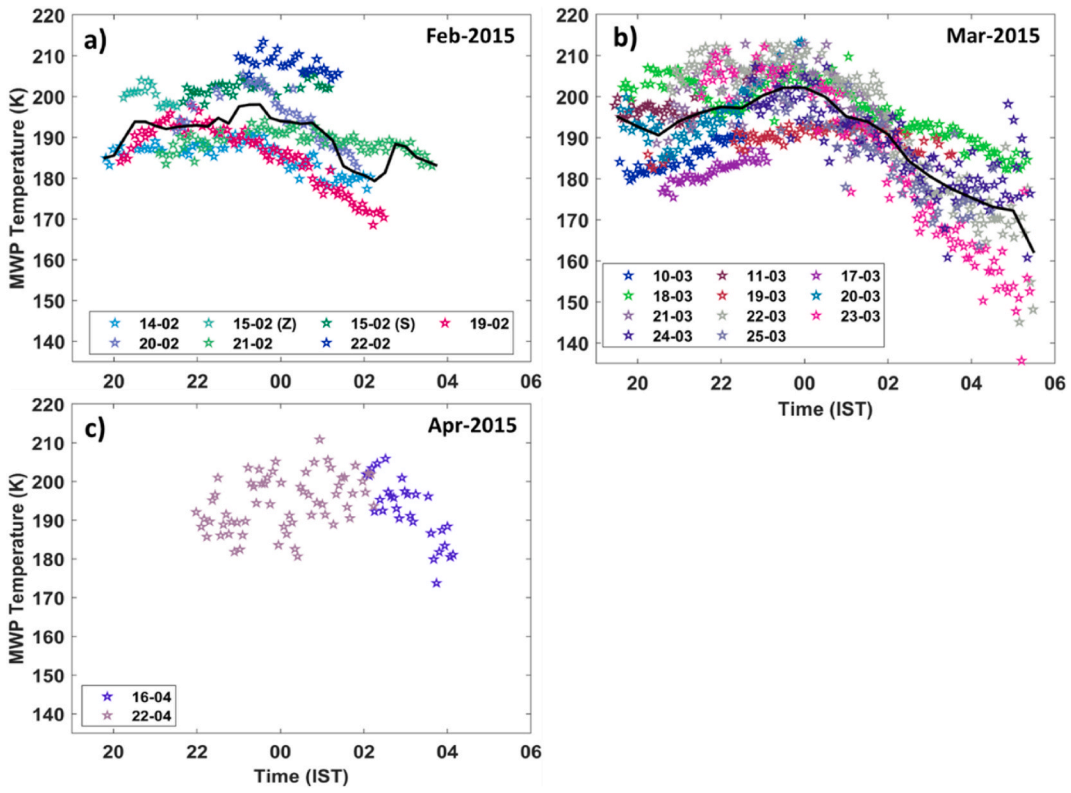

Fig. 7. Temporal variation of MWP temperatures on different nights during the study period. Different colored stars represent different nights as noted in the legend of each panel. The dates in the legend are in dd-mm format. The solid black line represents MTV for each month.

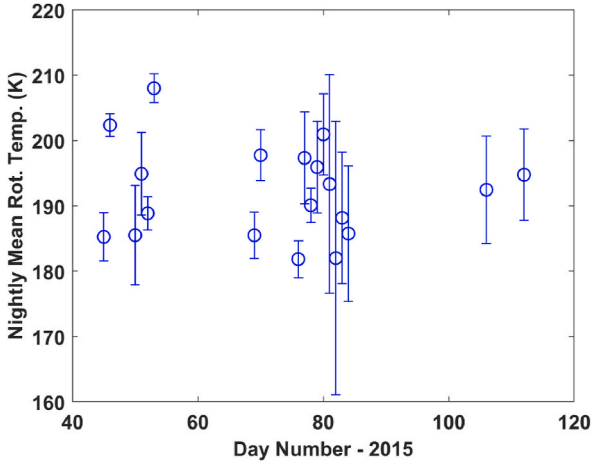

Fig. 8. Plot of nocturnal mean MWP temperatures with respect to day number in 2015. The open circles represent nocturnal mean MWP temperatures, while the vertical lines denote one standard deviation from the mean.

4.3.1. Comparison of temperature variabilities between the present work and previous studies

Several studies have examined the temporal variations of nocturnal OH band rotational temperatures (hereafter referred to as OH temperatures unless mentioned otherwise) in the low-latitude MLT region. However, research in the low-latitude sector, particularly the equatorial region, has not been as extensive as in the mid- and high-latitude sectors. Takahashi et al. (1974) conducted one of the first studies in the low-latitude sector at Cachoeira Paulista (22.7° S, 45.2° W) and observed significant day-to-day variability in OH temperatures. They reported nocturnal mean temperatures in the range of 160–200 K during July 1972–1973. Clemesha et al. (1990) identified an apparent semi-annual oscillation (SAO) in OH temperatures at Cachoeira Paulista during 1983–1986, with nocturnal mean temperatures between 185 K and 200 K during the spring season. Using data from the equatorial station Fortaleza (3.9° S, 38.4° W), Takahashi et al. (1994) observed strong seasonal variabilities and a pronounced SAO in OH temperatures, reporting nocturnal mean temperatures in the range of 200–225 K during spring at Fortaleza. In another study, Takahashi et al. (1998) noticed that the MTV of OH temperatures during spring peaks around 20:00 LT at Fortaleza and decreases monotonically afterward. Studies from the low-latitude station, Arecibo (18.4° N, 66.7° W) have shown that during winter, OH temperatures generally increase between evening and premidnight hours, followed by a gradual decrease during premidnight to postmidnight hours, and an increasing pattern in the early morning hours (Tepley et al., 1981; Zhou et al., 1997). Nocturnal mean temperatures in the range of 200–210 K were observed at Arecibo by Zhuo et al. (1997), while Tepley et al. (1981) reported spatial mean temperatures between 170 K and 250 K.

Past studies from the Indian low-latitude station Kolhapur (16.8° N, 74.2° E) indicate that OH temperatures either show a decreasing trend in the evening-premidnight sector and then remain almost constant for the rest of the night (Mukherjee and Parihar, 2004; Parihar and Mukherjee, 2008) or exhibit a decreasing pattern throughout the night (Parihar et al., 2013) during February–March. Occasionally, Parihar et al. (2013) observed that the decreasing trend reversed in the early morning hours at Kolhapur. Nocturnal mean OH temperatures were reported to be in the range of 190–210 K at Kolhapur during February and March (Mukherjee and Parihar, 2004; Parihar and Mukherjee, 2008). Taori et al. (2012a) analyzed OH temperatures from Gadanki (13.5° N, 79.2° E) during 2009–2011 and found monthly mean temperatures in the range of 190–210 K, with a peak around the spring equinox. In a study from the low-latitude station Pune (18.5° N, 73.8° E), Fadnavis et al. (2016) observed half-hourly mean OH temperatures between 160 K and 290 K. They noted both increasing and decreasing trends in the evening-premidnight sector and a decreasing trend after midnight.

It is evident from the previous two paragraphs that strong day-to-day variabilities are present in the nocturnal OH temperatures at low latitudes across all longitude sectors. The local time variation of individual or mean OH temperatures exhibits different patterns at different stations. The MTV of OH temperatures at Tirunelveli is similar to those reported by Tepley et al. (1981), Zhou et al. (1997), and Fadnavis et al. (2016). However, due to a lack of data, we could not verify the presence of any early morning increase in the OH temperatures during winter at Tirunelveli (i.e., February 2015) as reported by Tepley et al. (1981) and Zhou et al. (1997). During the months of our study, Tepley et al. (1981) and Fadnavis et al. (2016) observed peak OH temperatures around 21:00–22:00 LT, while we noticed a peak around midnight (i.e., 23:30 IST). It is interesting to note that the MTV of OH temperatures at Fortaleza, which is closest to Tirunelveli latitude-wise, is markedly different during the season of the present study. Therefore, it appears that the local time variation of OH temperatures does not have any apparent dependence on the latitude or longitude of observation at low latitudes.

Nocturnal mean OH temperatures obtained from Tirunelveli match very well with the values reported by Clemesha et al. (1990) from Cachoeira Paulista and by Mukherjee and Parihar (2004) and Parihar and Mukherjee (2008) from Kolhapur during the same season. Takahashi et al. (1994) found slightly higher nocturnal mean OH temperatures at Fortaleza compared to the present study, while Fadnavis et al. (2016) reported much higher nocturnal mean OH temperatures at Pune. These observations indicate that there is no apparent latitudinal dependence in the nocturnal mean OH temperatures in the low latitudes.

4.3.2. *Comparison between MWP and model temperatures*

In this work, we have utilized neutral temperatures at an altitude of 87 km obtained from the NRLMSISE-00 model. The altitude of 87 km is chosen as it is known to be the average peak altitude of the OH emission layer (Baker and Stair Jr, 1988). We have selected March 2015 for comparison as it has the maximum number of clear sky nights available within the study period, and MWP temperatures are available almost uniformly at all local times (Fig. 7b). Neutral temperatures were obtained from NRLMSISE-00 at 30 min intervals between 18:00 IST and 06:00 IST on all days in March 2015. The MTV of the NRLMSISE-00 temperatures was obtained by averaging all the temperatures available at each 30 min bin. A comparison between MWP and NRLMSISE-00 MTV shows an excellent match in the postmidnight sector (Fig. 9). A decreasing trend was observed in both sets of temperatures between midnight and early morning, though the temperature gradient was much larger for MWP in comparison to the NRLMSISE-00. The NRLMSISE-00 temperatures show a weak increasing trend in the morning hours (i.e., 05:00–06:00 IST), but half-hourly average MWP temperatures were either unreliable or unavailable during this period. A contrasting behavior was noticed between the MWP and NRLMSISE-00 MTV in the evening to premidnight sector. Differences between half-hourly average MWP and NRLMSISE-00 temperatures ranged from 8.5 to 29 K in the evening to premidnight sector and from 6.4 to 13 K in the early morning sector.

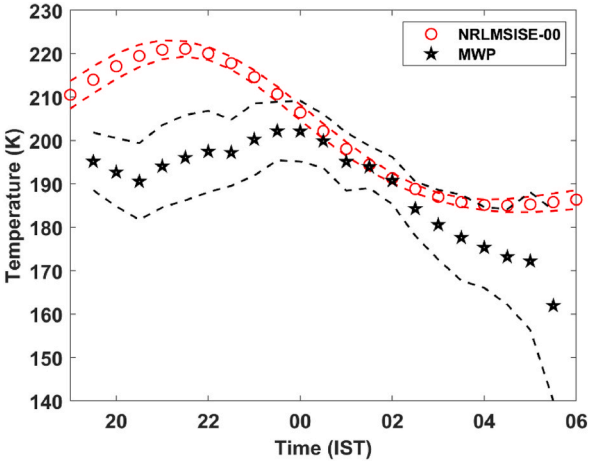

Fig. 9. Temporal variations of half-hourly mean temperatures obtained from MWP (black star) and NRLMSISE-00 (red open circle) model in March 2015. The black and red dashed lines denote one standard deviation from the MWP and NRLMSISE-00 mean temperatures, respectively.

Zhou et al. (1997) compared OH(6,2) rotational temperatures obtained at Arecibo in January 1993 with TIMEGCM model temperatures. Both temperatures showed similar temporal variations between evening and postmidnight, with a good match in their magnitudes. However, the model and observation showed contrasting behaviors in the early morning hours, with differences of up to 10 K. Mukherjee and Parihar (2004) observed that the temporal variation of OH(8,3) rotational temperatures at Kolhapur compared very well with MSIS-86 temperatures in March 2003. The magnitudes of both sets of temperatures also matched well, except in the early morning hours when differences of up to 20 K were seen. However, Fadnavis et al. (2016) reported a large difference of ~70 K between the OH(6,2) rotational temperatures and WACCM model temperatures at Pune in March 2013. In the present study, the observed and model temperatures compare well in the midnight to early morning hours, which is opposite to the general pattern seen in the previous comparison studies mentioned here. Solar activity levels were similar during March 2003, March 2013, and March 2015 (F10.7 index range: 120–150 solar flux units). However, the MTV of neutral temperatures obtained from the NRLMSISE-00 model in March 2015 differed considerably from the MSIS-86 and WACCM model outputs in March 2003 and March 2013, respectively. It is interesting to note that the MTV of MWP temperatures at Tirunelveli (Fig. 9) matches better with the MSIS-86 and WACCM model results in March. The reason (s) for the different behavior of the NRLMSISE-00 model compared to the other two models during the equinox (i.e., March) is not apparent and requires further study.

5. Conclusion

This study utilizes the P1 line intensities of the OH(6,2) band obtained with the Tirunelveli MWP for the first time. The line intensities and temperatures obtained with the MWP are validated by comparing them with co-located ASAI OH broadband intensities and SABER temperatures. The main findings of this study are noted below.

1) An excellent correlation between the Tirunelveli MWP and SABER temperatures is observed. The mean temperature difference (14.88 ± 4.31 K) between these two instruments is slightly larger than the values obtained by other researchers at different latitude sectors, except for Sau et al. (2024).
2) The small sample size (i.e., 5 nights) and the presence of a strong temperature inversion layer near the peak OH emission on all the nights could be plausible reasons for the slightly large mean temperature difference obtained in this study. However, the individual temperature differences reported here are within the range of individual temperature differences observed in several past studies (i.e., ±20.0 K).
3) The intensity of the P1 lines of the OH(6,2) band measured by the MWP matches very well with the OH broadband intensity obtained from the co-located ASAI. The MWP and ASAI reveal the same dominant periodicity in the OH(6,2) rotational temperatures and the OH broadband intensity.
4) The MTV of MWP temperatures exhibits an increasing (decreasing) trend before (after) midnight and a peak at ~23:30 IST in February and March 2015. Nocturnal mean MWP temperatures are observed in the range of 180–210 K, which matches well with previous reports from the Indian longitude sector.

5) The MTV of MWP and NRLMSISE-00 temperatures were similar (contrasting) in the midnight to early morning (evening to midnight) sector in March 2015. Temporal variation of the NRLMSISE-00 temperatures differed from the MSIS-86 and WACCM model temperatures in March for similar solar activity levels.
6) Comparing past results with our observations, no clear latitudinal and longitudinal dependence is observed in the local time variation and nocturnal mean of the rotational temperatures at low latitudes.

CRediT authorship contribution statement

Sukanta Sau: Writing – review & editing, Writing – original draft, Methodology, Investigation, Formal analysis, Data curation, Conceptualization. **S. Gurubaran:** Writing – review & editing, Supervision, Methodology. **V.L. Narayanan:** Writing – review & editing. **Dupinder Singh:** Writing – review & editing, Methodology. **S. Sripathi:** Writing – review & editing. **A.P. Dimri:** Writing – review & editing.

Data availability statement

The Tirunelveli MWP and ASAI data sets used in this work are available with the corresponding author and will be made available on request. http://saber.gats-inc.com/browse_data.php#https://ccmc.gsfc.nasa.gov/modelweb/models/nrlmsise00.php

Declaration of competing interest

The authors declare that they have no known competing financial interests or personal relationships that could have appeared to influence the work reported in this paper.

Acknowledgement

Research at the Indian Institute of Geomagnetism is funded by the Department of Science and Technology (DST), Government of India. We wish to thank the whole TIMED mission team for making the SABER data publicly available. The SABER data can be accessed from http://saber.gats-inc.com/browse_data.php#. NRLMSISE-00 simulation results have been provided by the Community Coordinated Modeling Center (CCMC) at Goddard Space Flight Center through their publicly available simulation services https://ccmc.gsfc.nasa.gov(https://ccmc.gsfc.nasa.gov/modelweb/models/nrlmsise00.php). The NRLMSISE-00 Model was developed by Douglas Drob and John Emmert at the Naval Research Laboratory, USA.

Data availability

Data will be made available on request.

References

Baker, D.J., Stair, Jr.A.T., 1988. Rocket measurements of the altitude distributions of the hydroxyl airglow. Phys. Scripta 37 (4), 611. https://doi.org/10.1088/0031-8949/37/4/021.

Clemesha, B.R., Takahashi, H., Batista, P.P., 1990. Mesopause temperatures at 23°S. J. Geophys. Res. Atmos. 95 (D6), 7677–7681. https://doi.org/10.1029/JD095iD06p07677.

Dawkins, E.C.M., Feofilov, A., Rezac, L., Kutepov, A.A., Janches, D., Höffner, J., Russell III, J., 2018. Validation of SABER v2.0 operational temperature data with ground-based lidars in the mesosphere-lower thermosphere region (75–105 km). J. Geophys. Res. Atmos. 123 (17), 9916–9934. https://doi.org/10.1029/2018JD028742.

Esplin, R., Mlynczak, M.G., Russell, J., Gordley, L., Team, T.S., 2023. Sounding of the atmosphere using broadband emission radiometry (SABER): Instrument and science measurement description. Earth Space Sci. 10 (9), e2023EA002999. https://doi.org/10.1029/2023EA002999.

Fadnavis, S., Beig, G., 2004. Mesospheric temperature inversions over the Indian tropical region. Ann. Geophys. 22 (10), 3375–3382. https://doi.org/10.5194/angeo-22-3375-2004.

Fadnavis, S., Feng, W., Shepherd, G.G., Plane, J.M.C., Sonbawne, S., Roy, C., Ghude, S.D., 2016. Preliminary observations and simulation of nocturnal variations of airglow temperature and emission rates at Pune (18.5°N), India. J. Atmos. Sol. Terr. Phys. 149, 59–68. https://doi.org/10.1016/j.jastp.2016.10.002.

García-Comas, M., Funke, B., Gardini, A., López-Puertas, M., Jurado-Navarro, A., von Clarmann, T., Sheese, P.E., 2014. MIPAS temperature from the stratosphere to the lower thermosphere: comparison of vM21 with ACE-FTS, MLS, OSIRIS, SABER, SOFIE and lidar measurements. Atmos. Meas. Tech. 7 (11), 3633–3651. https://doi.org/10.5194/amt-7-3633-2014.

García-Comas, M., López-Puertas, M., Marshall, B.T., Wintersteiner, P.P., Funke, B., Bermejo-Pantaleón, D., Russell III, J.M., 2008. Errors in sounding of the atmosphere using broadband emission radiometry (SABER) kinetic temperature caused by non-local-thermodynamic-equilibrium model parameters. J. Geophys. Res. Atmos. 113 (D24). https://doi.org/10.1029/2008JD010105.

Ghodpage, R.N., Taori, A., Gurav, O.B., Patil, P.T., Gurubaran, S., Siingh, D., Naniwadekar, G.P., 2019. Observation of mesospheric wave using collocated OH airglow temperature and radar wind measurements over Indian low latitude. Adv. Space Res. 64 (10), 1865–1875. https://doi.org/10.1016/j.asr.2019.04.029.

Guharay, A., Taori, A., Bhattacharjee, S., Pant, P., Pande, B., Pandey, K., 2009. First ground-based mesospheric measurements from central Himalayas. Curr. Sci. 97 (5), 664–669.

Krassovsky, V.I., Shefov, N.N., Yarin, V.I., 1962. Atlas of the airglow spectrum 3000–12400 Å. Planet. Space Sci. 9 (12), 883–915. https://doi.org/10.1016/0032-0633(62)90008-9.

Langhoff, S.R., Werner, H.J., Rosmus, P., 1986. Theoretical transition probabilities for the OH meinel system. J. Mol. Spectrosc. 118 (2), 507–529. https://doi.org/10.1016/0022-2852(86)90186-4.

Liu, W., Xu, J., Smith, A.K., Yuan, W., 2015. Comparison of rotational temperature derived from ground-based OH airglow observations with TIMED/SABER to evaluate the einstein coefficients. J. Geophys. Res.: Space Phys. 120 (11), 10069–10082. https://doi.org/10.1002/2015JA021886.

López-González, M.J., García-Comas, M., Rodríguez, E., López-Puertas, M., Shepherd, M. G., Shepherd, G.G., Wiens, R.H., 2007. Ground-based mesospheric temperatures at mid-latitude derived from O2 and OH airglow SATI data: Comparison with SABER measurements. J. Atmos. Sol. Terr. Phys. 69 (17), 2379–2390. https://doi.org/10.1016/j.jastp.2007.07.004.

Meriwether, J.W., 1975. High latitude airglow observations of correlated short-term fluctuations in the hydroxyl meinel 8-3 band intensity and rotational temperature. Planet. Space Sci. 23 (8), 1211–1221. https://doi.org/10.1016/0032-0633(75)90170-1.

Mertens, C.J., Mlynczak, M.G., López-Puertas, M., Wintersteiner, P.P., Picard, R.H., Winick, J.R., Russell III, J.M., 2001. Retrieval of mesospheric and lower thermospheric kinetic temperature from measurements of CO2 15 μm Earth limb emission under non-LTE conditions. Geophys. Res. Lett. 28 (7), 1391–1394. https://doi.org/10.1029/2000GL012189.

Mlynczak, M.G., Daniels, T., Hunt, L.A., Yue, J., Marshall, B.T., Russell III, J.M., Yee, J.-H., 2020. Radiometric stability of the SABER instrument. Earth Space Sci. 7 (2), e2019EA001011. https://doi.org/10.1029/2019EA001011.

Mukherjee, G.K., Parihar, N., 2004. Measurement of rotational temperature at Kolhapur, India. Ann. Geophys. 22 (9), 3315–3321. https://doi.org/10.5194/angeo-22-3315-2004.

Mulligan, F.J., Lowe, R.P., 2008. OH-equivalent temperatures derived from ACE-FTS and SABER temperature profiles – a comparison with OH*(3-1) temperatures from Maynooth (53.2° N, 6.4° W). Ann. Geophys. 26 (4), 795–811. https://doi.org/10.5194/angeo-26-795-2008.

Narayanan, V.L., Gurubaran, S., 2013. Statistical characteristics of high frequency gravity waves observed by OH airglow imaging from Tirunelveli (8.7°N). J. Atmos. Sol. Terr. Phys. 92, 43–50. https://doi.org/10.1016/j.jastp.2012.09.002.

Narayanan, V.L., Gurubaran, S., Emperumal, K., 2009a. A case study of a mesospheric bore event observed with an all-sky airglow imager at Tirunelveli (8.7°N). J. Geophys. Res. Atmos. 114 (D8). https://doi.org/10.1029/2008JD010602.

Narayanan, V.L., Gurubaran, S., Emperumal, K., 2009b. Imaging observations of upper mesospheric nightglow emissions from Tirunelveli (8.7°N). Indian J. Radio Space Phys. 38, 150–158.

Narayanan, V.L., Gurubaran, S., Emperumal, K., 2010. Airglow imaging observations of small-scale structures driven by convective instability in the upper mesosphere over Tirunelveli (8.7°N). J. Geophys. Res. Atmos. 115 (D19). https://doi.org/10.1029/2009JD012937.

Narayanan, V.L., Gurubaran, S., Emperumal, K., 2012. Nightglow imaging of different types of events, including a mesospheric bore observed on the night of February 15, 2007 from Tirunelveli (8.7°N). J. Atmos. Sol. Terr. Phys. 78–79, 70–83. https://doi.org/10.1016/j.jastp.2011.07.006.

Nozawa, S., Saito, N., Kawahara, T., Wada, S., Tsuda, T.T., Maeda, S., Johnsen, M.G., 2023. A statistical study of convective and dynamic instabilities in the polar upper mesosphere above Tromsø. Earth Planets Space 75 (1), 22. https://doi.org/10.1186/s40623-023-01771-1.

Oberheide, J., Offermann, D., Russell III, J.M., Mlynczak, M.G., 2006. Intercomparison of kinetic temperature from 15 μm CO2 limb emissions and OH*(3,1) rotational temperature in nearly coincident air masses: SABER, GRIPS. Geophys. Res. Lett. 33 (14). https://doi.org/10.1029/2006GL026439.

Parihar, N., Mukherjee, G.K., 2008. Measurement of mesopause temperature from hydroxyl nightglow at Kolhapur (16.8°N, 74.2°E), India. Adv. Space Res. 41 (4), 660–669. https://doi.org/10.1016/j.asr.2007.05.002.

Parihar, N., Singh, D., Gurubaran, S., 2017. A comparison of ground-based hydroxyl airglow temperatures with SABER/TIMED measurements over 23° N, India. Ann. Geophys. 35 (3), 353–363. https://doi.org/10.5194/angeo-35-353-2017.

Parihar, N., Taori, A., Gurubaran, S., Mukherjee, G.K., 2013. Simultaneous measurement of OI 557.7 nm, O_2 (0, 1) Atmospheric Band and OH (6, 2) Meinel band nightglow at

Kolhapur (17° N), India. Ann. Geophys. 31 (2), 197–208. https://doi.org/10.5194/angeo-31-197-2013.
Pendleton, Jr.W.R., Espy, P.J., Hammond, M.R., 1993. Evidence for non-local-thermodynamic-equilibrium rotation in the OH nightglow. J. Geophys. Res.: Space Phys. 98 (A7), 11567–11579. https://doi.org/10.1029/93JA00740.
Ramesh, K., Sridharan, S., Raghunath, K., Rao, S.V.B., 2017. A chemical perspective of day and night tropical (10°N–15°N) mesospheric inversion layers. J. Geophys. Res.: Space Phys. 122 (3), 3650–3664. https://doi.org/10.1002/2016JA023721.
Reid, I.M., 2024. Meteor radar for investigation of the MLT Region: a review. Atmosphere 15 (4), 505. https://doi.org/10.3390/atmos15040505.
Reid, I.M., Spargo, A.J., Woithe, J.M., Klekociuk, A.R., Younger, J.P., Sivjee, G.G., 2017. Seasonal MLT-region nightglow intensities, temperatures, and emission heights at a Southern Hemisphere midlatitude site. Ann. Geophys. 35 (3), 567–582. https://doi.org/10.5194/angeo-35-567-2017.
Russell, J., Mlynczak, M., Gordley, L., 1994. Overview of the Sounding of the Atmosphere Using Broadband Emission Radiometry (SABER) Experiment for the Thermosphere-Ionsphere-Mesosphere Energetics and Dynamics (TIMED) Mission, vol.2266. SPIE.
Sau, S., Terra, P., Brum, C.G.M., Vargas, F.A., Lautenbach, J., Gurubaran, S., 2024. Retrieval of rotational temperatures from the arecibo observatory ebert-fastie spectrometer and their inter-comparison with Co-Located K-Lidar and SABER measurements. Earth Space Sci. 11 (2), e2023EA003323. https://doi.org/10.1029/2023EA003323.
Scheer, J., 1995. What can be learned from rotational temperatures derived from ground-based airglow observations about the aeronomy of the southern hemisphere. Adv. Space Res. 16 (5), 61–69. https://doi.org/10.1016/0273-1177(95)00173-C.
Sivakandan, M., Kapasi, D., Taori, A., 2014. The occurrence altitudes of middle atmospheric temperature inversions and mesopause over low-latitude Indian sector. Ann. Geophys. 32 (8), 967–974. https://doi.org/10.5194/angeo-32-967-2014.
Smith, S.M., Baumgardner, J., Mertens, C.J., Russell, J.M., Mlynczak, M.G., Mendillo, M., 2010. Mesospheric OH temperatures: simultaneous ground-based and SABER OH measurements over Millstone Hill. Adv. Space Res. 45 (2), 239–246. https://doi-org.iigm.remotexs.in/10.1016/j.asr.2009.09.022.
Sridharan, R., Taori, A., Gurubaran, S., Rajaram, R., Shepherd, M.G., 1999. First results on daytime mesopause OH rotational temperatures using ground-based photometry from equatorial latitudes. J. Atmos. Sol. Terr. Phys. 61 (15), 1131–1142. https://doi.org/10.1016/S1364-6826(99)00062-0.
Takahashi, H., Clemesha, B.R., Sahai, Y., 1974. Nightglow OH (8, 3) band intensities and rotational temperature at 23°S. Planet. Space Sci. 22 (9), 1323–1329. https://doi.org/10.1016/0032-0633(74)90051-8.
Takahashi, H., Clemesha, B.R., Sahai, Y., Batista, P.P., 1994. Seasonal variations of the mesopause temperature observed at equatorial (4°S) and low (23°S) latitude stations. Adv. Space Res. 14 (9), 97–100. https://doi.org/10.1016/0273-1177(94)90122-8.
Takahashi, H., Gobbi, D., Batista, P.P., Melo, S.M.L., Teixeira, N.R., Buriti, R.A., 1998. Dynamical influence on the equatorial airglow observed from the South American sector. Adv. Space Res. 21 (6), 817–825. https://doi.org/10.1016/S0273-1177(97)00680-7.
Taori, A., Dashora, N., Raghunath, K., Russell III, J.M., Mlynczak, M.G., 2011. Simultaneous mesosphere-thermosphere-ionosphere parameter measurements over Gadanki (13.5°N, 79.2°E): first results. J. Geophys. Res.: Space Phys. 116 (A7). https://doi.org/10.1029/2010JA016154.
Taori, A., Kamalakar, V., Jayaraman, A., 2012a. First observation of upper mesospheric semi annual oscillations using ground based airglow measurements from Indian low latitudes. Adv. Space Res. 49 (5), 937–942. https://doi.org/10.1016/j.asr.2011.12.016.
Taori, A., Kamalakar, V., Raghunath, K., Rao, S.V.B., Russell, J.M., 2012b. Simultaneous Rayleigh lidar and airglow measurements of middle atmospheric waves over low latitudes in India. J. Atmos. Sol. Terr. Phys. 78–79, 62–69. https://doi.org/10.1016/j.jastp.2011.06.012.
Taylor, M.J., Taori, A.K., Hatch, D.R., Liu, H.L., Roble, R.G., 2005. Characterization of the semi-annual-oscillation in mesospheric temperatures at low-latitudes. Adv. Space Res. 35 (11), 2037–2043. https://doi.org/10.1016/j.asr.2005.05.111.
Tepley, C.A., Burnside, R.G., Meriwether, J.W., 1981. Horizontal thermal structure of the mesosphere from observations of OH(8-3) band emissions. Planet. Space Sci. 29 (11), 1241–1249. https://doi.org/10.1016/0032-0633(81)90129-X.
Vineeth, C., Pant, T.K., Sridharan, R., 2011. Daytime upper mesospheric energetics over a tropical station, Trivandrum (8.5°N, 77°E): an investigation using the multiwavelength dayglow photometry. J. Geophys. Res.: Space Phys. 116 (A1). https://doi.org/10.1029/2010JA015633.
von Savigny, C., McDade, I.C., Eichmann, K.U., Burrows, J.P., 2012. On the dependence of the OH* Meinel emission altitude on vibrational level: SCIAMACHY observations and model simulations. Atmos. Chem. Phys. 12 (18), 8813–8828. https://doi.org/10.5194/acp-12-8813-2012.
Wiens, R.H., Moise, A., Brown, S., Sargoytchev, S., Peterson, R.N., Shepherd, G.G., Rodrigo, R., 1997. SATI: a spectral airglow temperature imager. Adv. Space Res. 19 (4), 677–680. https://doi.org/10.1016/S0273-1177(97)00162-2.
Yue, X., Friedman, J.S., Zhou, Q., Wu, X., Lautenbach, J., 2019. Long-term lidar observations of the gravity wave activity near the mesopause at Arecibo. Atmos. Chem. Phys. 19 (5), 3207–3221. https://doi.org/10.5194/acp-19-3207-2019.
Zhou, Q.H., Sulzer, M.P., Tepley, C.A., Fesen, C.G., Roble, R.G., Kelley, M.C., 1997. Neutral winds and temperature in the tropical mesosphere and lower thermosphere during January 1993: observation and comparison with TIME-GCM results. J. Geophys. Res.: Space Phys. 102 (A6), 11507–11519. https://doi.org/10.1029/97JA00439.